nanomaterials

MDPI

Article

Efficient Analysis of Small Molecules via Laser Desorption/Ionization Time-of-Flight Mass Spectrometry (LDI–TOF MS) Using Gold Nanoshells with Nanogaps

Noori Kim [1,†], Yoon-Hee Kim [1,†], Gaon Jo [1], Jin Yoo [1], Seung-min Park [2,3], Bong-Hyun Jun [1,*] and Woon-Seok Yeo [1,*]

[1] Department of Bioscience and Biotechnology, Konkuk University, Seoul 05029, Republic of Korea; bobbysen@naver.com (N.K.); yoonhees@konkuk.ac.kr (Y.-H.K.); jogaon883@gmail.com (G.J.); jin4261624@gmail.com (J.Y.)
[2] Department of Urology, Stanford University School of Medicine, Stanford, CA 94305, USA; sp293@stanford.edu
[3] School of Chemistry, Chemical Engineering and Biotechnology, Nanyang Technological University, Singapore 639798
* Correspondence: bjun@konkuk.ac.kr (B.-H.J.); wsyeo@konkuk.ac.kr (W.-S.Y.)
† These authors contributed equally to this work.

Abstract: Matrix-assisted laser desorption/ionization time-of-flight mass spectrometry (MALDI–TOF MS) is a commonly used technique for analyzing large biomolecules. However, the utilization of organic matrices limits the small-molecule analysis because of the interferences in the low-mass region and the reproducibility issues. To overcome these limitations, a surface-assisted laser desorption/ionization (SALDI), which utilizes nanostructured metallic surfaces, has been developed. Herein, a novel approach for SALDI–MS was proposed using silica@gold core–shell hybrid materials with a nanogap-rich shell (SiO_2@Au NGS), which is an emerging material due to its excellent heat-generating capabilities. The gold shell thickness was controlled by adjusting the concentration of gold precursor for the growth of gold nanoparticles. SALDI-MS measurements were performed on a layer formed by drop-casting a mixture of SiO_2@Au NGS and analytes. At the optimized process, the gold shell thickness was observed to be 17.2 nm, which showed the highest absorbance. Based on the enhanced SALDI capability, SiO_2@Au NGS was utilized to detect various small molecules, including amino acids, sugars, and flavonoids, and the ionization softness was confirmed with a survival yield upon fragmentation. The limits of detection, reproducibility, and salt tolerance of SiO_2@Au NGS demonstrate its potential as an effective and reliable SALDI material for small-molecule analyses.

Keywords: matrix-assisted laser desorption/ionization time-of-flight mass spectrometry; gold nanoshell; nanogap; surface-assisted laser desorption/ionization; silica core nanoparticle; small-molecule analysis

Citation: Kim, N.; Kim, Y.-H.; Jo, G.; Yoo, J.; Park, S.-m.; Jun, B.-H.; Yeo, W.-S. Efficient Analysis of Small Molecules via Laser Desorption/Ionization Time-of-Flight Mass Spectrometry (LDI–TOF MS) Using Gold Nanoshells with Nanogaps. *Nanomaterials* **2024**, *14*, 25. https://doi.org/10.3390/nano14010025

Academic Editor: Alain Pignolet

Received: 24 October 2023
Revised: 27 November 2023
Accepted: 12 December 2023
Published: 21 December 2023

1. Introduction

Matrix-assisted laser desorption/ionization time-of-flight (MALDI–TOF) mass spectrometry (MS) is widely used for the analysis of large biomolecules, such as proteins and oligonucleotides, using an organic matrix for soft ionization [1–3]. Following the pioneering studies of Tanaka et al., who utilized a metal powder dispersed in glycerol [4,5], and Karas and Hillenkamp, who employed a small organic molecule as a matrix [6], various types of organic matrices, including 2,5-dihydroxybenzoic acid, sinapinic acid, α-cyano-4-hydroxycinnamic acid, and 2,4,6-trihydroxyacetophenone, are commonly used for this purpose depending on the analyte type. MALDI–TOF MS is an effective bioanalytical tool for biomolecules because of its simple and fast operating processes, high tolerance to biological contaminants, and the ability to facilitate multiple analyses simultaneously.

However, the necessity of using an organic matrix considerably limits its practical application (particularly for small-molecule analyses) because of the interferences in the low-mass region. In addition, the solvents utilized for dissolving the analyte and matrix, the co-crystallization of the matrix and analyte, and even the deposition method strongly affect the shot-to-shot and sample-to-sample reproducibility of this technique. To overcome these limitations, significant efforts have been devoted to developing an organic matrix-free analysis method known as surface-assisted laser desorption/ionization (SALDI), which is primarily based on the use of nanostructured surfaces and inorganic nanoparticles (NPs) instead of the organic matrix [7,8]. Since the pioneering study of Tanaka, who employed 30 nm cobalt NPs dispersed in glycerol for lysozyme analysis [5], various nanomaterials based on metals, including Au, Ag, TiO_2, Zn, and Pt, have been applied for SALDI–MS [9]. Furthermore, carbon-based materials, such as graphite, carbon nanotubes, graphene oxide (GO), and graphene derivatives, have been actively used for this purpose [10–12]. In particular, inorganic NPs, including gold nanoparticles (AuNPs) [13] and silver NPs [14], are widely employed in SALDI–MS because of their advantageous physiochemical properties, photothermal activities, and simple fabrication procedures affording homogeneously controllable morphologies; however, the use of these NPs raises issues such as maintaining colloidal stability during analysis and heat dissipating after laser irradiation owing to their high thermal conductivity. Therefore, several attempts have been made to obtain efficient SALDI substrates by confining the laser-driven energy to nanoscale gap structures. As a result, substrates with closely packed nanostructures fabricated via vapor deposition [15] and droplet deposition [16] were produced. The SALDI efficiency and signal strength of these substrates were strongly correlated with their sub-micrometer and nanometer-scale morphologies, which could be controlled by adjusting the sputtered metal amount and the number of deposition cycles. However, fabricating homogeneous nanogap structures via these methods is difficult owing to the bulk agglomerate formation and uncontrolled interparticle aggregation during the deposition process.

Recently, "gold nanoshells", core–shell NPs consisting of silica NP cores and AuNP surfaces, were utilized for the first time as a SALDI substrate by Jinrui et al. [17]. Such materials can effectively confine heat by the silica core NPs and abundant "hot spots" distributed across the interparticle junctions of the closely packed AuNPs on the silica surface. The existence of correlations between the SALDI signals of various analytes and the thickness of gold nanoshells were discussed in detail by Mingyi et al. [18]. They prepared three types of gold nanoshells and compared their SALDI efficiencies, which depended on the surface coverage and shell roughness at the nanometer scale. The optimized gold nanoshells with the highest SALDI efficiency have been successfully applied in the mass spectrometry imaging of the mouse brain. In these applications, gold nanogap structures generated "hot spots", which consisted of the highly localized regions of an intense electromagnetic field due to plasmonic coupling between adjacent nanostructures. Recently, we have prepared gold nanogap shells using silica NPs, which significantly amplified a local electromagnetic field [19,20]. Finely controlled nanogap structures were obtained by increasing the shell thickness, which in turn decreased the average nanogap size from approximately 4 to 1 nm. Although these NPs were utilized as substrates and catalysts for surface-enhanced Raman scattering spectroscopy, they have not been employed for SALDI yet. Herein, we propose an organic matrix-free LDI–MS method using silica@gold core–shell hybrid nanocomposites with nanogap-rich shell (SiO_2@Au NGS) structure. SiO_2@Au NGS with various shell thicknesses and well-ordered surface structures were synthesized by modulating the Au precursor concentration during growth.

2. Experimental Section

2.1. Chemicals

Quercetin hydrate, cellobiose, triethylene glycol, tetraethylene glycol, tetraethyl orthosilicate (TEOS), gold (III) chloride, polyvinylpyrrolidone (PVP, average molecular weight: ~10,000), (3-aminopropyl) trimethoxysilane (APTS), and ascorbic acid were pur-

chased from Sigma–Aldrich (St. Louis, MO, USA). Glutamic acid, mannitol, serine, galactose, histidine, and aqueous ammonium hydroxide (NH_4OH, 25–28%) were procured from Daejung Chemical & Metals Co., Ltd. (Gyeonggi-do, Republic of Korea). Aspartic acid and acetonitrile were acquired from Junsei Chemical Co., Ltd. (Tokyo, Japan). Kaempferol hydrate and pentaethylene glycol were purchased from the Tokyo Chemical Industry (Tokyo, Japan). Tryptophan, arginine, and glutamine were procured from Samchun Chemicals Co., Ltd. (Gyeonggi-do, Republic of Korea). Absolute ethanol was obtained from Merck (Darmstadt, Germany). GO was purchased from Graphene Laboratories Inc. (Ronkonkoma, NY, USA). Benzyl pyridinium salt was prepared using a method previously reported by Tang et al. [21]. Deionized water was obtained using an AquaMAX Ultra 370 water purification system (Younglin Instruments, Anyang, Republic of Korea).

2.2. Synthesis of SiO_2@Au NGS

AuNPs were prepared using tetrakis (hydroxymethyl) phosphonium chloride (THPC) as a reducing agent. First, a NaOH solution (0.2 M, 1.5 mL) was diluted with deionized water (47.5 mL), followed by the sequential addition of THPC (80%, 12 µL) and gold (III) chloride (50 mM, 1 mL) solutions. The obtained mixture was vigorously stirred for 1 h. AuNP-seed-immobilized silica NPs (SiO_2@Au) were synthesized using a silica NP template. Silica NPs were prepared via the Stöber process [22]. Briefly, TEOS (1.6 mL) was mixed with ethanol (40 mL), followed by the addition of the NH_4OH solution (3–5.5 mL) to obtain silica NPs of various sizes. The reaction mixture was stirred vigorously for 1 h at 60 °C and then for 19 h at 25 °C. The produced solution was washed several times with ethanol via centrifugation at 9000× *g*. The resulting silica NPs (15 mg) were modified with amino groups by stirring with the APTS (15.5 µL) and NH_4OH (10 µL) solutions in a vortex mixer for 12 h. The mixture was washed several times with ethanol via centrifugation at 9000× *g*, and the obtained aminated silica NPs (2 mg) were mixed with the AuNP solution (10 mL) overnight. After washing with deionized water, the resulting dark-brown pellets were dispersed in ethanol. SiO_2@Au NGS were synthesized through the seed-mediated growth of SiO_2@Au at different concentrations of the gold precursor solution. Briefly, SiO_2@Au (10 mg) was dispersed in an aqueous PVP solution and stirred at 500 rpm. During stirring, 200 µL of a 50 mM Au^{3+} aqueous solution and 100 mM ascorbic acid aqueous solution were added simultaneously at 5 min intervals. The addition of the precursor solutions was repeated to achieve a final Au^{3+} concentration of 0.5, 1.0, 1.5, or 2 mM. The obtained mixture was washed with deionized water and redispersed in ethanol.

2.3. Characterization

Transmission electron microscopy (TEM) images were captured using JEM-1010 (JEOL, Tokyo, Japan) and JEM-2010 (JEOL, Tokyo, Japan) instruments with acceleration voltages of 80 and 120 kV, respectively. The UV–visible absorption spectra were recorded using a single-beam UV/visible spectrophotometer (U-5100, HITACHI, Tokyo, Japan).

2.4. MALDI-TOF MS Analysis of Small Molecules

To prepare the samples for LDI–TOF MS analyses, 100 µM stock solutions of small molecules were produced. The amino acids and sugars were dissolved in distilled water, and oligoethylene glycols and flavonoids were dissolved in ethanol. SiO_2@Au $NGS_{0.5–2.0}$ (10 µL, 1 mg/mL in ethanol) were mixed with the analyte solutions (5 µL) at various concentrations, and the obtained mixtures (1.5 µL) were pipetted onto stainless-steel 384-well target plates (Bruker Daltonics, Bremen, Germany). The prepared samples were dried under a vacuum at 25 °C and analyzed directly via MS. The MALDI–TOF MS analyses were performed using an Autoflex III MALDI–TOF mass spectrometer (Bruker Daltonics, Germany) equipped with a smart beam laser (λ = 355 nm) serving as an ionization source. All spectra were acquired in a positive mode at an accelerating voltage of 19 kV and a repetition rate of 50 Hz with an average number of shots equal to ~500.

3. Results and Discussions

3.1. Preparation and Characterization of SiO_2@Au NGS

The fabrication process of SiO_2@Au NGS is illustrated in Figure 1. SiO_2@Au NGS was synthesized in two steps, including the attachment of AuNP seeds to silica NPs and the seed-mediated growth of AuNP seeds. To attach AuNPs to the substrate surface, silica NPs (~178 nm) were aminated with APTS. Then, the aminated silica NPs were mixed with AuNPs (~3 nm) to prepare the AuNP seed-immobilized silica NPs. Subsequently, gold precursor solutions with different concentrations were added to grow AuNP seeds, resulting in SiO_2@Au NGS. The SiO_2@Au NGS morphology was controlled by varying the concentration of the Au^{3+} precursor in the reaction mixture during the growth process, as shown in the corresponding transmission electron microscopy (TEM) images (Figure 1a–f). The thickness of the gold shell was averaged from the equivalent spherical diameter of 30 AuNPs that constitute the outer gold shell. By varying the concentration of Au^{3+} precursors as 0, 0.5, 1.0, 1.5, and 2.0 mM, shell thicknesses of each particle were measured as 2.3 ± 0.4, 8.3 ± 1.6, 11.9 ± 2.6, 13.1 ± 2.4, and 17.2 ± 2.0 nm (SiO_2@Au $NGS_{0.5–2.0}$). Notably, the shell thickness affected not only the nanogap size but also plasmonic absorption properties. Characteristic plasmonic frequencies of the SiO_2@Au NGS with different Au^{3+} concentrations were observed in their absorption spectra recorded in the ultraviolet (UV)/visible range (Figure S1). When using a higher concentration of the Au^{3+} precursor, we found uncontrolled growth of individual AuNPs, and therefore, we could not obtain NGS materials. In addition, we presume that nanogap structures on the surface would not be afforded at higher concentrations of the Au^{3+} precursor because of the coalescence among AuNPs. To evaluate the laser irradiation absorption properties of various SiO_2@Au NGS samples during LDI, their absorbances at 355 nm are compared in Figure 1f. The absorbance gradually increases with increasing Au^{3+} concentration from 0 to 1.5 mM, and a slight increase in absorbance is observed at 2.0 mM. These structural and optical characteristics can be used to predict the desorption efficiency during LDI spectrometry using the laser-driven energy for the desorption and ionization of analytes.

3.2. Matrix Properties of SiO_2@Au $NGS_{0.5\sim2.0}$ Evaluated Using Small Molecules

To utilize the prepared SiO_2@Au NGS as a matrix for LDI–TOF spectrometry, a layer of SiO_2@Au NGS was formed by drop-casting a mixture of colloidal SiO_2@Au NGS and target analytes, and desorption and ionization of these analytes were performed by irradiating the resulting layer with a pulsed laser beam (Scheme 1). We examined the feasibility of utilizing SiO_2@Au $NGS_{0.5–2.0}$ as matrices for LDI–TOF MS analysis and their efficiency by studying various small molecules, including amino acid serine, sugar mannitol, quercetin, and pentaethylene glycol.

The analytes were dissolved in distilled water or ethanol, considering their solubility differences, and the resulting solutions were mixed with the synthesized SiO_2@Au $NGS_{0.5}$, SiO_2@Au $NGS_{1.0}$, SiO_2@Au $NGS_{1.5}$, and SiO_2@Au $NGS_{2.0}$. AuNP seed-immobilized silica NPs (SiO_2@Au NGS_0) produced without seed-mediated gold growth were used as a control. Five representative mass spectra recorded for each of the four analytes are shown in Figure 2, and their detailed peak assignments with peak intensities, signal-to-noise (S/N) ratios, and resolutions are summarized in Table S1. In general, the adduct ion peaks corresponding to the studied analytes are clearly observed in Figure 2, and their intensities increase with increasing concentration of the gold precursor solution during the SiO_2@Au NGS synthesis. Except while using quercetin, the peak intensities of SiO_2@Au $NGS_{2.0}$ are higher than those of SiO_2@Au $NGS_{1.5}$, although SiO_2@AuNG$S_{2.0}$ and SiO_2@AuNG$S_{1.5}$ have a similar absorption peak at 355 nm—by a factor of 4 for serine, 25 for mannitol, and 10 for pentaethylene glycol. We presumed that the surface area of the embedded gold shell nanostructures with nanogaps on the silica surface increased with increasing gold precursor concentration to facilitate the accommodation of the energy supplied by laser irradiation and its subsequent transfer to the analytes, which increased the SALDI efficiency. In addition, the enhanced plasmonic properties of SiO_2@Au NGS and rapid

heating due to the low thermal conductivity of the silica NP core significantly enhanced the SALDI effect. In summary, SiO_2@Au $NGS_{2.0}$ exhibited the optimal matrix properties among the four gold shell materials, and we further validated the versatility of this material for LDI–MS by analyzing various small molecules and comparing it with other well-known SALDI materials.

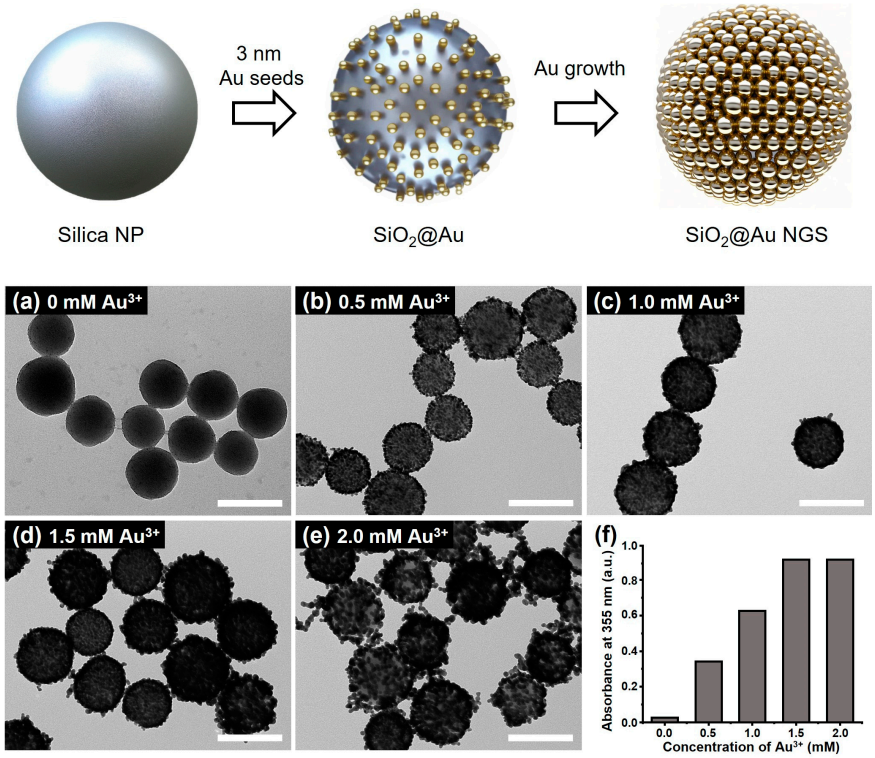

Figure 1. Schematics of the SiO_2@Au NGS preparation through the seed-mediated growth, and TEM images of SiO_2@Au NGS obtained after the growth of AuNP seeds at gold precursor concentrations of (**a**) 0, (**b**) 0.5, (**c**) 1.0, (**d**) 1.5, and (**e**) 2.0 mM. (**f**) Absorption values at 355 nm correspond to each SiO_2@Au NGS. Inset scale bars of (**a**–**e**) indicate 200 nm.

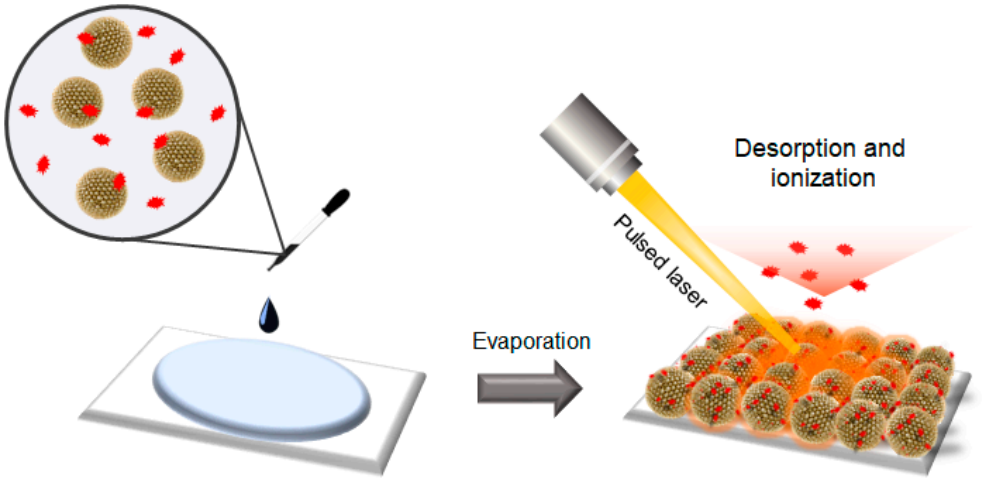

Scheme 1. Schematics of the detection of target analytes via the SiO_2@Au NGS-assisted LDI technique.

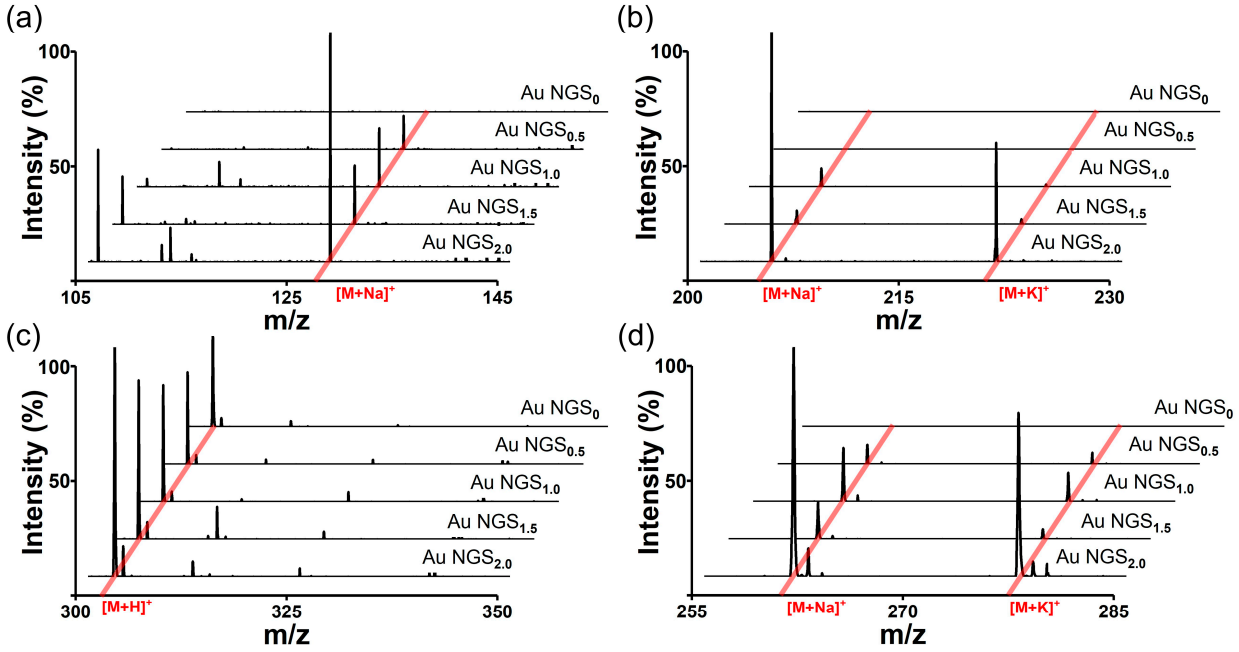

Figure 2. LDI–TOF mass spectra of small molecules obtained for the SiO_2@Au $NGS_{0–2.0}$ matrices: (**a**) serine, (**b**) mannitol, (**c**) quercetin, and (**d**) pentaethylene glycol.

3.3. Analyses of Small Molecules and Their Mixtures

Next, we analyzed various small molecules using SiO_2@Au $NGS_{2.0}$ to evaluate the matrix properties of the synthesized material. Four classes of small molecules were examined: amino acids (aspartic acid, glutamic acid, and glutamine), oligoethylene glycols (triethylene glycol and tetraethylene glycol), sugars (mannitol and galactose), and flavonoids (quercetin and kaempferol). Analytical solutions for LDI–MS analysis were prepared using distilled water for amino acids and sugars and ethanol for oligoethylene glycols and flavonoids. As shown in Figure 3, the SALDI spectra of SiO_2@Au $NGS_{2.0}$ exhibit distinct strong peaks corresponding to the adduct ions of amino acids (a–c), oligoethylene glycols (d,e), sugars (f,g), and flavonoids (h,i) with high intensities and S/N ratios without any significant background interferences (detailed peak assignment is provided in Table S2). Note that a gold peak is observed at m/z = 197. Subsequently, mixtures of small molecules were tested to confirm the separation of each analyte from the mixed samples. We prepared mixed samples containing three amino acids (glutamine, histidine, and arginine), three oligoethylene glycols (triethylene glycol, tetraethylene glycol, and pentaethylene glycol), three sugars (galactose, mannitol, and cellobiose), and three molecules from different classes (tryptophan, quercetin, and cellobiose). The mass spectra of each analyte mixture also clearly show major peaks corresponding to the adduct ions of the studied analytes with weak background peaks (Figure 4; for detailed peak assignment, see Table S3). These results strongly suggest that the nanoengineered gold shells with nanogaps on the silica surface SiO_2@Au $NGS_{2.0}$ with well-ordered surface structures are a highly effective SALDI material for the analysis of various small molecules and their mixtures.

3.4. Limits of Detection (LODs) and Reproducibility

LODs were measured for three analytes (glutamine, cellobiose, and kaempferol) to evaluate the practical feasibility of the SiO_2@Au $NGS_{2.0}$-based LDI technique. The LODs obtained at S/N ratios higher than six were 37.5 pmole for glutamine, 7.5 fmole for cellobiose, and 75 fmole for kaempferol (Figure 5). These values are comparable to those determined in previous studies using gold-based materials [13,23]. We also investigated the reproducibility of the fabricated material via multiple mass determinations (n = 25) for cellobiose (100 pmole in 1 μL on the target plate). The calculated relative standard

deviation of 18.6% was comparable to or better than the values obtained in other studies using AuNPs (Figure S2) [24].

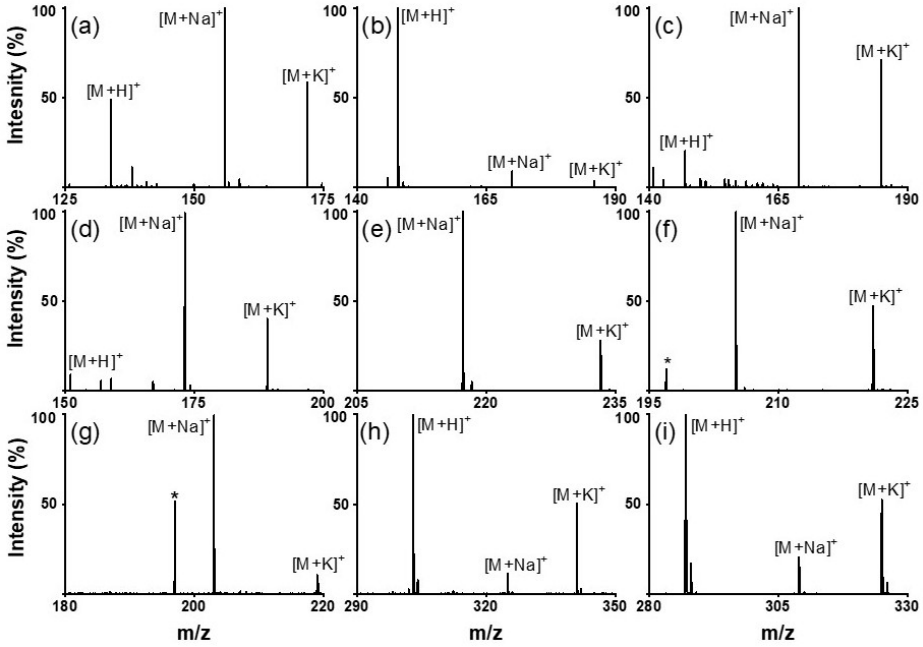

Figure 3. LDI–TOF mass spectra of amino acids: ((**a**) aspartic acid, (**b**) glutamic acid, and (**c**) glutamine); oligoethylene glycols: ((**d**) triethylene glycol and (**e**) tetraethylene glycol); sugars: ((**f**) mannitol and (**g**) galactose); and flavonoids: ((**h**) quercetin and (**i**) kaempferol) obtained using the SiO_2@Au $NGS_{2.0}$ matrix. *: matrix.

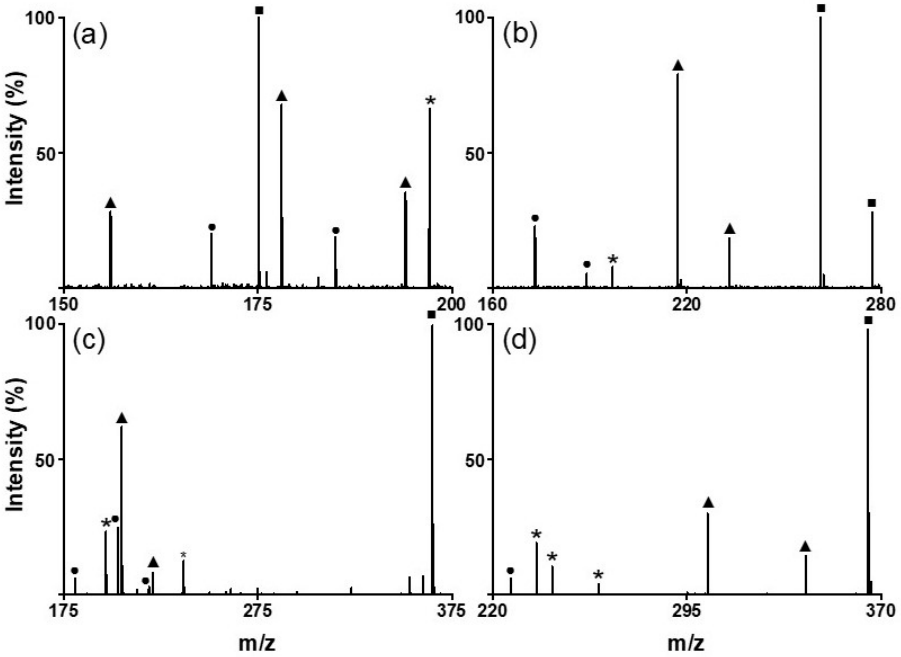

Figure 4. LDI–TOF mass spectra obtained for the mixtures of (**a**) amino acids (●: Glutamine, ▲: histidine, and ■: arginine), (**b**) oligoethylene glycols (●: triethylene glycol, ▲: tetraethylene glycol, and ■: pentaethylene glycol), (**c**) sugars (●: galactose, ▲: mannitol, and ■: cellobiose), and (**d**) sugar (●: tryptophan, ▲: quercetin, and ■: cellobiose) using the SiO_2@Au $NGS_{2.0}$ matrix. *: matrix.

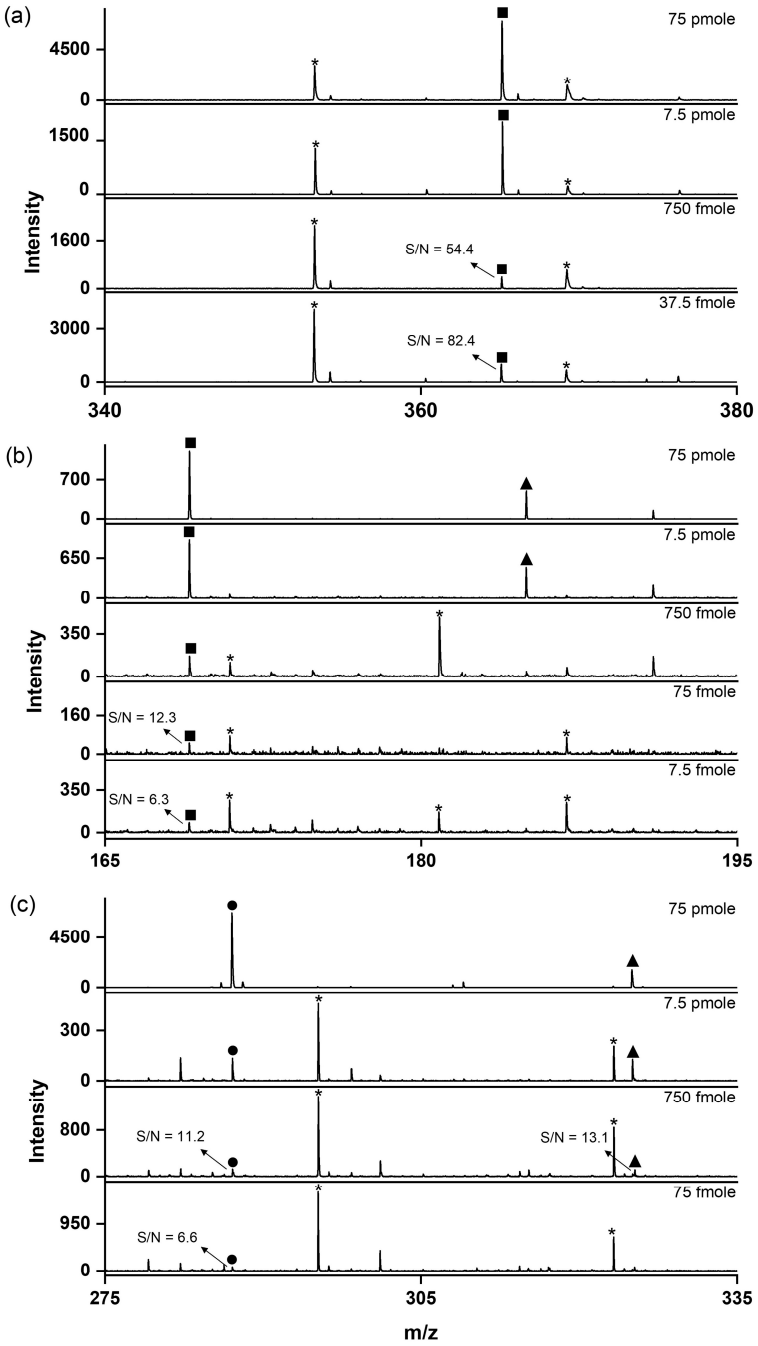

Figure 5. LDI–TOF mass spectra recorded to determine the LODs of small molecules using the SiO_2@Au $NGS_{2.0}$ matrix: (**a**) glutamine, (**b**) cellobiose, and (**c**) kaempferol. ●: $[M+H]^+$, ■: $[M+Na]^+$, ▲: $[M+K]^+$, and *: matrix.

3.5. Comparison of AuNP, GO, and SiO_2@Au NGS Matrices

The superiority of SiO_2@Au $NGS_{2.0}$ as a SALDI matrix over other commonly used inorganic matrices, AuNPs and GO was verified by comparing their SALDI properties using four analytes: kaempferol, cellobiose, triethylene glycol, and serine. The mass spectra obtained for AuNPs, GO, and SiO_2@Au $NGS_{2.0}$ are shown in Figure 6, and a detailed peak assignment is provided in Table S4. The GO spectrum exhibited kaempferol peaks with the highest intensity compared to the intensities of the three compounds but with very poor resolution, whereas the other three analytes were negligibly observed. AuNPs showed peaks with decent intensities and S/N ratios for four analytes. Particularly for kaempferol analysis, peak intensities, S/N ratios, and resolutions obtained using

AuNPs were comparable to or better than those obtained using SiO_2@Au $NGS_{2.0}$. For cellobiose, triethylene glycol and serine, SiO_2@Au $NGS_{2.0}$ generated the most intense analyte peaks with higher S/N ratios and resolution with fewer background signals than AuNPs. We also examined the background signals in a higher range up to ~500 for kaempferol and cellobiose, and we found AuNPs afforded more background signals than SiO_2@Au $NGS_{2.0}$ (Figure S3). Furthermore, we examined the applicability of SiO_2@Au $NGS_{2.0}$ as a SALDI matrix using benzylpyridinium (BP) salt, which has been adopted as a "chemical thermometer" to investigate the ion desorption efficiency and internal energy transfer by measuring a survival yield (SY) [21]. BP is fragmented via laser irradiation during the LDI process to produce benzylic carbocations (Figure 7a); therefore, the SY of BP is an important parameter characterizing the SALDI efficiency and ionization "softness". The SY was calculated by dividing the ion intensity of the intact BP precursor by the sum of the intact BP and fragmented product intensities after LDI–MS measurements. Five SALDI analyses were conducted for BP using AuNPs, GO, and SiO_2@Au $NGS_{2.0}$ under the same experimental conditions. The obtained representative spectra are shown in Figure 6b. The average SY values determined from the five mass spectra (0.63 for AuNPs, 0.41 for GO, and 0.64 for SiO_2@Au $NGS_{2.0}$) imply that the ion desorption and internal energy transfer efficiency of AuNP is comparable to SiO_2@Au $NGS_{2.0}$; however, the standard deviation for SiO_2@Au $NGS_{2.0}$ (0.04) much better than those for other materials (0.16 for AuNPs and 0.20 for GO).

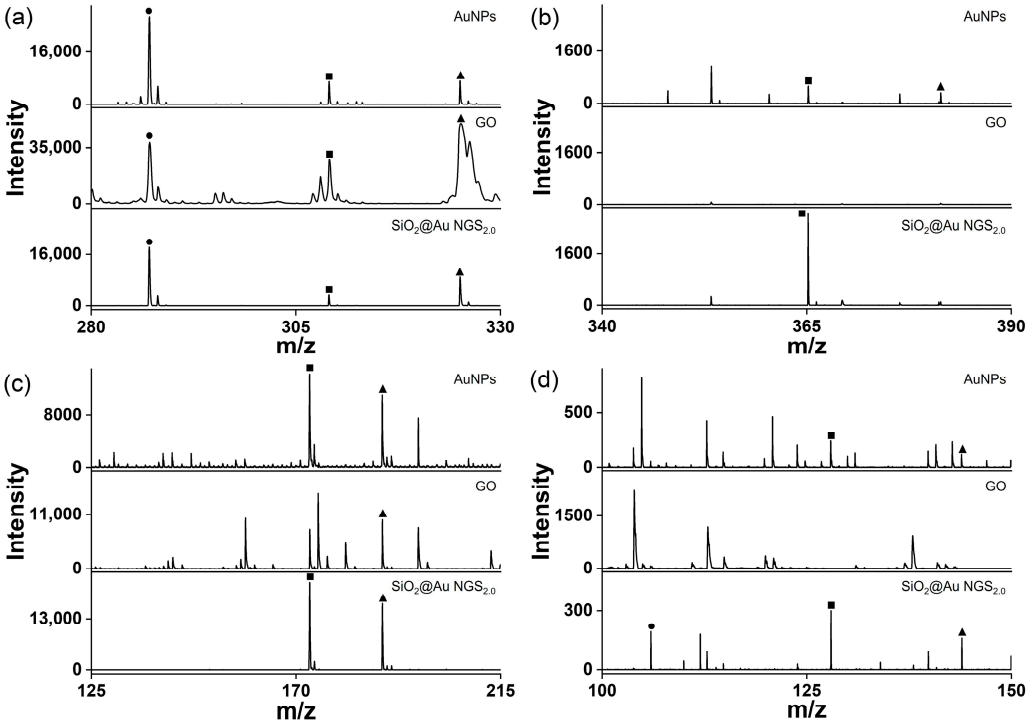

Figure 6. LDI–TOF mass spectra of small molecules obtained using the AuNP, GO, and SiO_2@Au $NGS_{2.0}$ matrices: (**a**) kaempferol, (**b**) cellobiose, (**c**) triethylene glycol, and (**d**) serine. ●: $[M+H]^+$, ■: $[M+Na]^+$, and ▲: $[M+K]^+$.

Another major issue encountered during the MALDI analysis is the signal suppression for analytes with salt contaminants (typically 150 mM NaCl) [25]. Therefore, SALDI materials must maintain colloidal stability during analysis (particularly when using salt-containing samples) and be tolerant to high salt concentrations [26]. As shown in Figure S4, SiO_2@Au $NGS_{2.0}$ showed excellent colloidal stability in NaCl solutions with concentrations up to 1 M, whereas AuNPs lost their stability at 50 mM or higher NaCl concentration. We also tested two analytes, histidine and mannitol, to investigate the salt tolerance of

SiO_2@Au $NGS_{2.0}$. The analytes were prepared in NaCl solutions at concentrations ranging from 0.1 to 1 M and then examined using SiO_2@Au $NGS_{2.0}$. The SALDI spectra of histidine clearly show the main peaks of the sodium adduct ($[M+Na]^+$) at m/z = 178.06 and sodiated sodium adduct ($[M+2Na–H]^+$) at m/z = 200.56 (Figure 8a). For mannitol, a sodium adduct peak (m/z = 205.07, $[M+Na]^+$) was observed as the main peak (Figure 8b). For both analytes, SiO_2@Au $NGS_{2.0}$ generated sodium adduct peaks as the main peaks at NaCl concentrations up to 1 M, indicating a high salt tolerance of the SALDI material; however, the peak intensities decreased with increasing salt concentration. For comparison, we also performed the SADLI analysis with AuNPs in high salt concentration. Unlike SiO_2@Au $NGS_{2.0}$, most SALDI spectra showed highly intense gold background peaks (m/z = 197), whereas analyte peaks were observed with low intensity and hardly observable at higher salt concentrations, which can account for the low colloidal stability of AuNPs compared to SiO_2@Au $NGS_{2.0}$ (Figure S5).

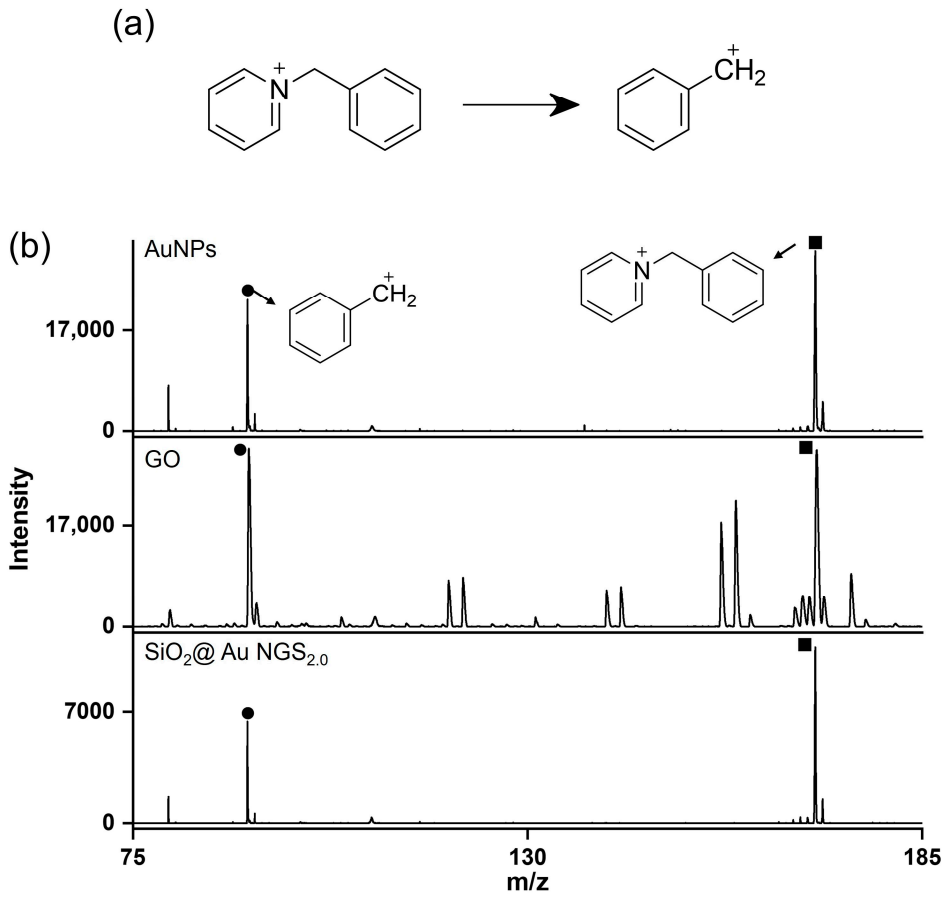

Figure 7. LDI–TOF mass spectra recorded during BP analysis. (**a**) Fragmentation reaction of BP during LDI–TOF measurements, and (**b**) representative LDI–TOF mass spectra obtained using the AuNP, GO, and SiO_2@Au $NGS_{2.0}$ matrices. •: Fragment and ■: BP.

Taken all together, the results and discussion above in terms of peak intensities, resolutions, S/N ratios, background signals, SY values, colloidal stability, and salt tolerance clearly indicate the superiority of SiO_2@Au $NGS_{2.0}$ as a SALDI matrix over other commonly used inorganic matrices, AuNPs and GO.

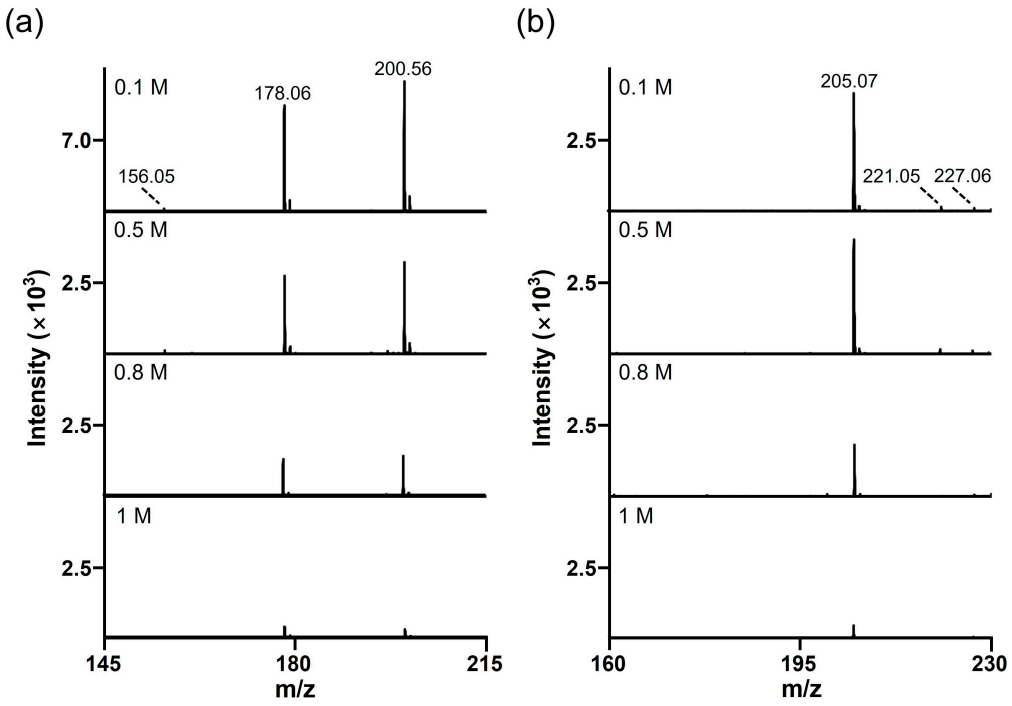

Figure 8. Salt tolerance of the SiO_2@Au $NGS_{2.0}$ matrix. Studied analytes (1 mM) were mixed with the NaCl solutions of various concentrations ranging between 0.1 and 1 M. (**a**) Histidine (m/z = 178.06, $[M+Na]^+$ and m/z = 200.56, $[M+2Na-H]^+$). (**b**) Mannitol (m/z = 205.07, $[M+Na]^+$; m/z = 221.05, $[M+K]^+$; and m/z = 227.06, $[M+2Na–H]^+$).

4. Conclusions

In summary, nanoengineered gold shells with nanogaps on the silica surface were utilized for the SALDI–MS analysis of small molecules. As the gold shell thickness increased, the plasmonic absorption of the SiO_2@Au NGS increased gradually, while maintaining its well-ordered nanogap structure. In addition, the signal intensity and S/N ratio of the SALDI-MS peaks also exhibited a similar correlation with the gold shell thickness of SiO_2@Au NGS. The phenomenon is presumed to be because of the high UV absorbance, which is advantageous for heat generation and contributes to the desorption of the analyte. Based on the excellent SALDI performance of SiO_2@Au $NGS_{2.0}$, various small molecules, including amino acids, sugars, flavonoids, and their mixtures, were investigated. This material demonstrated high reproducibility and salt tolerance, and its LODs were comparable to or better than those of other SALDI materials. Therefore, the material fabricated in this study can potentially replace the matrix-free LDI–MS analytical tools currently used by researchers.

Supplementary Materials: The following supporting information can be downloaded at https://www.mdpi.com/article/10.3390/nano14010025/s1, Figure S1: Absorption spectra of SiO_2@Au NGS; Figure S2: Signal variation of cellobiose; Figure S3: Raw data with mass range to ~500 for Figure 6a (kaempferol) and Figure 6b (cellobiose); Figure S4: Comparison of colloidal stability in NaCl solutions between SiO_2@Au $NGS_{2.0}$ and AuNPs; Figure S5: Salt tolerance of the AuNP matrix in NaCl solutions of various concentrations; Table S1: Detailed peak assignments for mass spectra in Figure 2; Table S2: Detailed peak assignments for mass spectra in Figure 3; Table S3: Detailed peak assignments for mass spectra in Figure 4; Table S4: Detailed peak assignments for mass spectra in Figure 6.

Author Contributions: Conceptualization, B.-H.J. and W.-S.Y.; methodology, N.K., Y.-H.K., G.J. and J.Y.; software, N.K., G.J. and Y.-H.K.; validation, S.-m.P., B.-H.J. and W.-S.Y.; formal analysis, N.K. and Y.-H.K.; investigation, N.K., Y.-H.K., G.J. and J.Y.; resources, N.K. and Y.-H.K.; data curation, N.K. and Y.-H.K.; writing—original draft preparation, N.K. and Y.-H.K.; writing—review and editing, S.-m.P.,

B.-H.J. and W.-S.Y.; visualization, Y.-H.K.; supervision, B.-H.J. and W.-S.Y.; project administration, B.-H.J. and W.-S.Y.; funding acquisition, B.-H.J. and W.-S.Y. All authors have read and agreed to the published version of the manuscript.

Funding: This research was supported by the National Research Foundation of Korea (NRF), funded by the Korean government (MSIT) [grant number NRF-2022R1A2C1006152], Ministry of Science and ICT [grant number NRF-2022R1A2C2012883], and Ministry of Trade, Industry, and Energy (MOTIE) of the Republic of Korea [grant number 20018608].

Data Availability Statement: The data presented in this study are available on request from the corresponding author.

Conflicts of Interest: The authors declare no conflict of interest.

References

1. Hale, J.E.; Butler, J.P.; Knierman, M.D.; Becker, G.W. Increased Sensitivity of Tryptic Peptide Detection by MALDI-TOF Mass Spectrometry Is Achieved by Conversion of Lysine to Homoarginine. *Anal. Biochem.* **2000**, *287*, 110–117. [CrossRef] [PubMed]
2. Gut, I.G. DNA Analysis by MALDI-TOF Mass Spectrometry. *Hum. Mutat.* **2004**, *23*, 437–441. [CrossRef] [PubMed]
3. Clark, A.E.; Kaleta, E.J.; Arora, A.; Wolk, D.M. Matrix-Assisted Laser Desorption Ionization-Time of Flight Mass Spectrometry: A Fundamental Shift in the Routine Practice of Clinical Microbiology. *Clin. Microbiol. Rev.* **2013**, *26*, 547–603. [CrossRef] [PubMed]
4. Tanaka, K. The Origin of Macromolecule Ionization by Laser Irradiation (Nobel Lecture). *Angew. Chem. Int. Ed.* **2003**, *42*, 3860–3870. [CrossRef] [PubMed]
5. Tanaka, K.; Waki, H.; Ido, Y.; Akita, S.; Yoshida, Y.; Yoshida, T. *Protein and Polymer Analyses up to Mlz 100,000 by Laser Ionization Time-of-Flight Mass Spectrometry*; Wiley: Hoboken, NJ, USA, 1988; Volume 2.
6. Karas, M.; Hillenkamp, F. Laser Desorption Ionization of Proteins with Molecular Masses Exceeding 10,000 Daltons. *Anal. Chem.* **1988**, *60*, 2299–2301. [CrossRef] [PubMed]
7. Watanabe, T.; Kawasaki, H.; Yonezawa, T.; Arakawa, R. Surface-Assisted Laser Desorption/Ionization Mass Spectrometry (SALDI-MS) of Low Molecular Weight Organic Compounds and Synthetic Polymers Using Zinc Oxide (ZnO) Nanoparticles. *J. Mass. Spectrom.* **2008**, *43*, 1063–1071. [CrossRef] [PubMed]
8. Song, K.; Cheng, Q. Desorption and Ionization Mechanisms and Signal Enhancement in Surface Assisted Laser Desorption Ionization Mass Spectrometry (SALDI-MS). *Appl. Spectrosc. Rev.* **2020**, *55*, 220–242. [CrossRef]
9. Chiang, C.K.; Chen, W.T.; Chang, H.T. Nanoparticle-Based Mass Spectrometry for the Analysis of Biomolecules. *Chem. Soc. Rev.* **2011**, *40*, 1269–1281. [CrossRef]
10. Law, K.P.; Larkin, J.R. Recent Advances in SALDI-MS Techniques and Their Chemical and Bioanalytical Applications. *Anal. Bioanal. Chem.* **2011**, *399*, 2597–2622. [CrossRef]
11. Lim, A.Y.; Ma, J.; Boey, Y.C.F. Development of Nanomaterials for SALDI-MS Analysis in Forensics. *Adv. Mater.* **2012**, *24*, 4211–4216. [CrossRef]
12. Kang, H.; Yun, H.; Lee, S.W.; Yeo, W.S. Analysis of Small Biomolecules and Xenobiotic Metabolism Using Converted Graphene-like Monolayer Plates and Laser Desorption/Ionization Time-of-Flight Mass Spectrometry. *Talanta* **2017**, *168*, 240–245. [CrossRef] [PubMed]
13. Su, C.L.; Tseng, W.L. Gold Nanoparticles as Assisted Matrix for Determining Neutral Small Carbohydrates through Laser Desorption/Ionization Time-of-Flight Mass Spectrometry. *Anal. Chem.* **2007**, *79*, 1626–1633. [CrossRef] [PubMed]
14. Cha, S.; Song, Z.; Nikolau, B.J.; Yeung, E.S. Direct Profiling and Imaging of Epicuticular Waxes on Arabidopsis Thaliana by Laser Desorption/ Ionization Mass Spectrometry Using Silver Colloid as a Matrix. *Anal. Chem.* **2009**, *81*, 2991–3000. [CrossRef] [PubMed]
15. Kurita, M.; Arakawa, R.; Kawasaki, H. Silver Nanoparticle Functionalized Glass Fibers for Combined Surface-Enhanced Raman Scattering Spectroscopy (SERS)/Surface-Assisted Laser Desorption/Ionization (SALDI) Mass Spectrometry: Via Plasmonic/Thermal Hot Spots. *Analyst* **2016**, *141*, 5835–5841. [CrossRef] [PubMed]
16. Hinman, S.S.; Chen, C.Y.; Duan, J.; Cheng, Q. Calcinated Gold Nanoparticle Arrays for On-Chip, Multiplexed and Matrix-Free Mass Spectrometric Analysis of Peptides and Small Molecules. *Nanoscale* **2016**, *8*, 1665–1675. [CrossRef]
17. Gan, J.; Wei, X.; Li, Y.; Wu, J.; Qian, K.; Liu, B. Designer SiO2@Au Nanoshells towards Sensitive and Selective Detection of Small Molecules in Laser Desorption Ionization Mass Spectrometry. *Nanomedicine* **2015**, *11*, 1715–1723. [CrossRef] [PubMed]
18. Du, M.; Chen, D.; Chen, Y.; Huang, Y.; Ma, L.; Xie, Q.; Xu, Y.; Zhu, X.; Chen, Z.; Yin, Z.; et al. Plasmonic Gold Nanoshell-Assisted Laser Desorption/Ionization Mass Spectrometry for Small-Biomolecule Analysis and Tissue Imaging. *ACS Appl. Nano Mater.* **2022**, *5*, 9633–9645. [CrossRef]
19. Seong, B.; Bock, S.; Hahm, E.; Huynh, K.H.; Kim, J.; Lee, S.H.; Pham, X.H.; Jun, B.H. Synthesis of Densely Immobilized Gold-assembled Silica Nanostructures. *Int. J. Mol. Sci.* **2021**, *22*, 2543. [CrossRef]
20. Bock, S.; Choi, Y.S.; Kim, M.; Yun, Y.; Pham, X.H.; Kim, J.; Seong, B.; Kim, W.; Jo, A.; Ham, K.M.; et al. Highly Sensitive Near-Infrared SERS Nanoprobes for in Vivo Imaging Using Gold-Assembled Silica Nanoparticles with Controllable Nanogaps. *J. Nanobiotechnology* **2022**, *20*, 130. [CrossRef]

21. Tang, H.W.; Ng, K.M.; Lu, W.; Che, C.M. Ion Desorption Efficiency and Internal Energy Transfer in Carbon-Based Surface-Assisted Laser Desorption/Ionization Mass Spectrometry: Desorption Mechanism(s) and the Design of SALDI Substrates. *Anal. Chem.* **2009**, *81*, 4720–4729. [CrossRef]
22. Stober, W.; Fink, A.; Ernst Bohn, D. Controlled Growth of Monodisperse Silica Spheres in the Micron Size Range. *J. Colloid Interface Sci.* **1968**, *26*, 62–69. [CrossRef]
23. Lee, J.; Lee, J.; Chung, T.D.; Yeo, W.S. Nanoengineered Micro Gold Shells for LDI-TOF Analysis of Small Molecules. *Anal. Chim. Acta* **2012**, *736*, 1–6. [CrossRef] [PubMed]
24. Wu, H.P.; Su, C.L.; Chang, H.C.; Tseng, W.L. Sample-First Preparation: A Method for Surface-Assisted Laser Desorption/Ionization Time-of-Flight Mass Spectrometry Analysis of Cyclic Oligosaccharides. *Anal. Chem.* **2007**, *79*, 6215–6221. [CrossRef] [PubMed]
25. Chen, R.; Xu, W.; Xiong, C.; Zhou, X.; Xiong, S.; Nie, Z.; Mao, L.; Chen, Y.; Chang, H.C. High-Salt-Tolerance Matrix for Facile Detection of Glucose in Rat Brain Microdialysates by Maldi Mass Spectrometry. *Anal. Chem.* **2012**, *84*, 465–469. [CrossRef]
26. Wen, X.; Dagan, S.; Wysocki, V.H. Small-Molecule Analysis with Silicon-Nanoparticle-Assisted Laser Desorption/Ionization Mass Spectrometry. *Anal. Chem.* **2007**, *79*, 434–444. [CrossRef]